Preliminary CANREB Beamline Commissioning Results

A. Mahon[1] and S. Saminathan[2]

[1]*McGill University, Montréal, Québec, H3A 2T8, Canada*
[2]*TRIUMF, Vancouver, British Columbia, V6T 2A3, Canada*
(Dated: September 5, 2019)

Commissioning of the CANREB (CANadian Rare isotope facility with Electron Beam ion source) at TRIUMF has recently begun through the EBIS (Electron Beam Ion Source) injection/extraction beamline. Throughout commissioning it is essential to have a means of verifying beam quality and ensuring that the required beam parameters along the beamline are met. This is accomplished using Tomography reconstruction, which consists of taking one-dimensional (1-D) scans at different projections and reconstructing an image of the beam in two-dimensions (2-D) using the MENT (Maximum ENTropy) algorithm. Tomography enables the visualization of the shape of the beam as well as the investigation into the possible presence of aberrations. The Tomography studies performed throughout this project focus primarily on the properties of the Test Ion source, the emittance through the RFQ (Radio Frequency Quadrupole) and the beam intensity measured by the Faraday Cups, all in order to ensure that the elements in the beamline function properly.

INTRODUCTION

The Advanced Rare IsotopE Laboratory (ARIEL) is one of TRIUMF's latest innovations, with the goal of tripling isotope production through the addition of two new production targets. This will allow for the optimization of experiment time, as multiple experiments will be able to use beam simultaneously. An essential component of this new project is the CANadian Rare isotope facility with Electron Beam ion source (CANREB) beamline, whose ground floor layout can be seen in Figure 1.
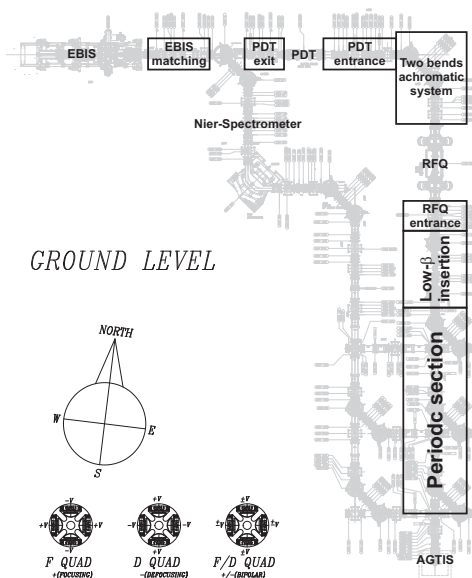

FIG. 1: Ground floor layout of the CANREB beamline.

As presented at the 2017 ICIS Conference, "CANREB will complement the presently used ECRIS based charge state breeder system by providing higher purity beams and extending the available mass range. Ions are first sent through a high resolution mass separator, where most of the isobaric contaminants can be removed. After this, the ions are injected into an RFQ cooler buncher and finally bunches are injected into an EBIS for charge state breeding" [1]. The Nier Spectrometer will then be used to select ions based on their m/q ratio, and send the beam on to the experimental areas.

The commissioning of this beamline began in February of 2019 using a test ion source producing stable alkaline Cs^{1+} ions with energy up to 60keV. The beam has successfully travelled through the injection line of the EBIS (AGTIS to PDT exit), however due to unforeseen complications with the EBIS, there has been little to no beam through the extraction region.

Throughout commissioning it is essential to have a means of verifying beam quality and ensuring that the required beam parameters along the beamline are met. The technique used to accomplish this is Tomography reconstruction. To generalize, this process consist of of taking one-dimensional (1-D) beam current profiles at different projections and reconstructing an image of the beam in two-dimensions (2-D). This is done by using the Maximum ENTropy (MENT) algorithm, which takes the measured profile data and their corresponding transfer matrices, and outputs many processed data files [2]. This output data can be used to reconstruct the 2-D contour plot desired.

Tomography can be performed in both real space and phase-space, with the specific procedure differing slightly for each case. This process enables the visualization of the shape of the beam, the investigation into the possible presence of aberrations. It also allows for the computation of essential beam parameters, such as the root mean squared (RMS) size as well as the emmittance. Pre-existing scripts were available to help perform the Tomography; throughout this project they were generalized and improved in order to facilitate this process. New scripts were also developed to address new data analysis requirements. In the following section the procedure for performing Tomography reconstruction will be explained in further depth.

TOMOGRAPHY PROCEDURE

The two main tools used to collect the necessary data for Tomography are Profile Monitors (PMs) and Linear Profile Monitors (LPMs), whose schematics can be seen in Figures 23 and 24 in the Appendix. Typically these measurement tools are located just past a triplet of quadrupoles, whose settings can be varied to manipulate the beam as desired (focus/defocus, steering, etc). A schematic of one such layout is shown in Figure 2.
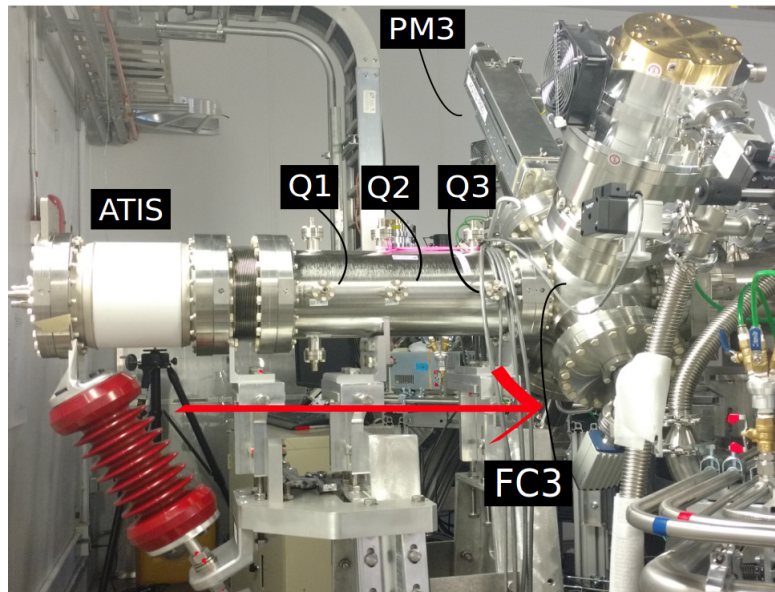

FIG. 2: Layout of the AGTIS source region. From left to right: ARIEL Test Ion source (ATIS), Quadrupole triplet (Q1, Q2, Q3) and PM3. Red arrow indicates the direction the beam travels.

Real space Tomography

In the case of real space Tomography, it is necessary to scan the beam in three distinct planes: vertical, horizontal and rotational. The diagnostics tool capable of doing so is the PM. This scan yields three profiles, which can be plotted using the python script *profiles_v2.py* (Example shown in Appendix, Figure 22). This script is also used to filter and smooth the data, although another version, *PM_functions_for_tomo.py* is more often called upon in the scripts to come, as it performs the same steps without the plots.

In order to reconstruct these 1-D profiles in 2-D, the well established Maximum ENTropy (MENT) algorithm is used. The script *PM_create_tomo_in.py* is used to create the input file necessary for this algorithm; it appends the wires' respective rotational transfer matrices with the smooth, filtered data. This input file is named *for_tomo.dat*. After having processed the data through the algorithm, the script *compare_input_output.py* is used to ensure that the MENT output matches the input profiles. Certain input Tomography values can be varied using the *in* file to improve the algorithm's matching, such as the number of iterations, the smoothing factor, the contour limits, and so on. Once the optimal matching has been achieved, it is possible to plot the contours generated by the algorithm and obtain a

2D image of the beam using the script *general_contour_plot.py*. These real space contour plots demonstrate the shape of the beam for the specified beam settings and can identify if there are any aberrations present.

Phase-space Tomography

The process for phase-space Tomography reconstruction is more complex than that of real space. First, a series of scans must be taken, where two quadrupoles within the triplet are kept at a fixed voltage value the entire time, and the third is varied between its minimum and maximum voltage in steps. This can be done using either a PM or a LPM as only the data from the horizontal and vertical planes are required. Once these scans are collected, the script *PM_integral_and_parab.py* is used to plot the $2\times RMS$ squared values of each scan as a function of voltage.

This is an essential step in the phase-space reconstruction, as the plots generated from this script assist in the selection of the specific range used for the Tomography. It is imperative that the points follow the general shape of a parabola and that the minimum point of the parabola is present and included in the range used for Tomography. It is also during this step that outlier points are removed from the chosen range.

The next step is to generate the transfer matrices for each different quadrupole scan. This is done using the beam optics module TRANSOPTR, written in FORTRAN, where it is necessary to input the correct quadrupole and $2\times RMS$ parameters into both the *data.dat* and *sy.f* scripts. One transfer matrix needs to be generated for each of the scan settings. Once all the matrix files are generated the script *PM_for_emit.py* is used to append them to their corresponding data file for both the x-plane and the y-plane, thus generating two input files for MENT, *for_tomo_x.dat* and *for_tomo_y.dat*. The algorithm is then run for each plane individually, and again it is important to verify if the input matched the output using *compare_input_output.py*. Once this is confirmed, the phase-space image is generated again using a slightly modified version of *general_contour_plot.py* script.

TEST ION SOURCE STUDIES

The test ion source used throughout the commissioning of CANREB was designed and manufactured internally at TRIUMF, and produces stable alkaline Cs^{1+} ions [3]. It is important to take a look at the source beam properties before it passes through the various other machine elements, therefore this was a main focus of the project. Simulations were first performed by previous co-op student Owen Lailey, whose results can be found in reference [4]. The procedures for Tomography reconstruction outlined in the previous section are now used to study the behaviour of the beam at the head of the beamline, just upstream of the test ion source. The beam envelope at this location can be seen in Figure 3.
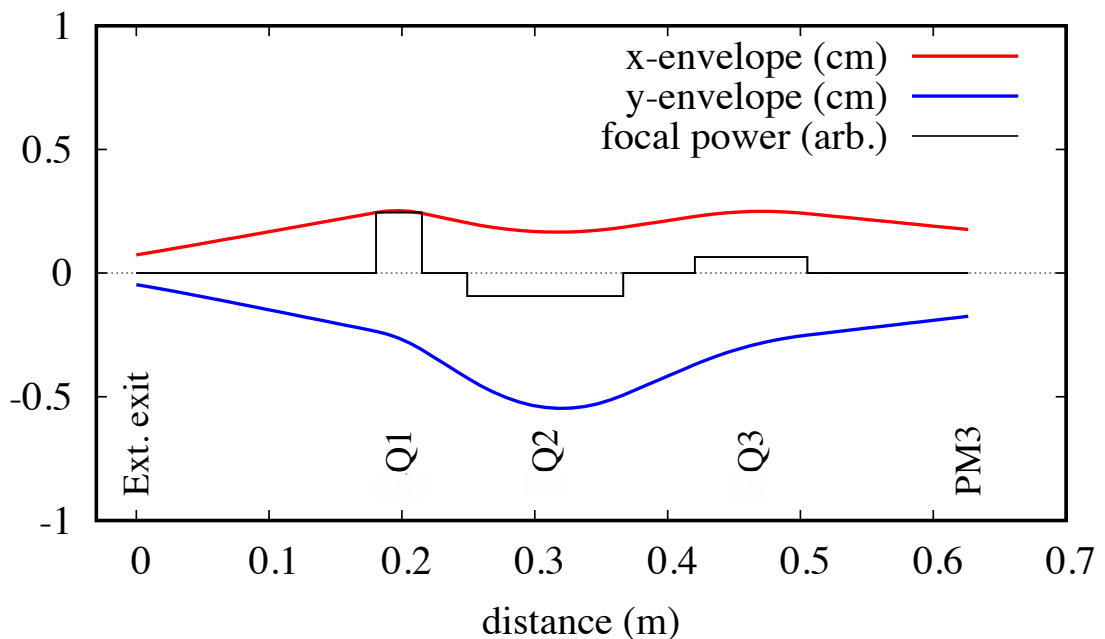

FIG. 3: Calculated beam envelope in the region of the Test Ion Source

Real space Tomography

In the beginning of the commissioning process, the source energy is kept at/below 30 keV, only half of its maximum capacity. Real space Tomography is performed at the location PM3, with the input and (MENT) output profiles being shown in Figure 4, where there is a very nice agreement between the two. The final Tomography image is shown in Figure 5; for the specified quadrupole settings the beams produced are almost perfectly round, which can be determined both visually and by the very similar $2 \times RMS$ values.
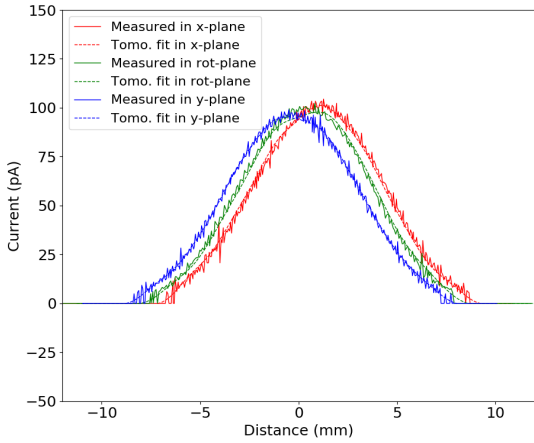
FIG. 4: Measured profiles (input) with MENT fit profiles (output) for real space.
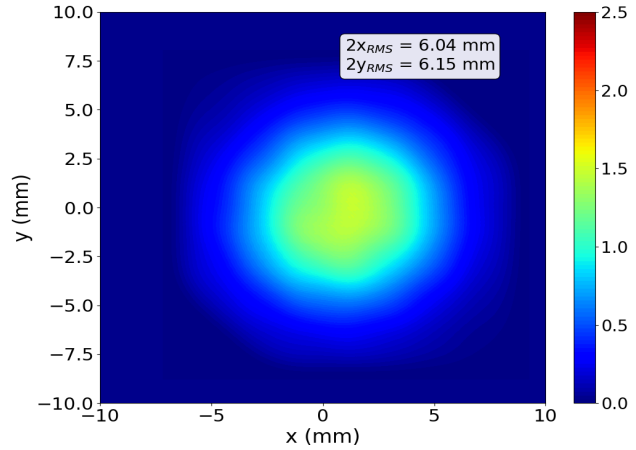
FIG. 5: Real space Tomography at the location PM3 for beams with AGTIS:Bias of 30 keV and Q1 = Q2 = Q3 = 0 V. Computed $2 \times RMS$ values printed on plot with colorbar indicated the intensity scale.

As the commissioning process advances, the source is ramped up to its full capacity of 60 keV, and real space Tomography is performed once again for various AGTIS:Bias voltages. The resulting $2 \times RMS$ values are plotted in Figure 6, which shows that as the beam energy is increased, the $2 \times RMS$ sizes decrease as expected.
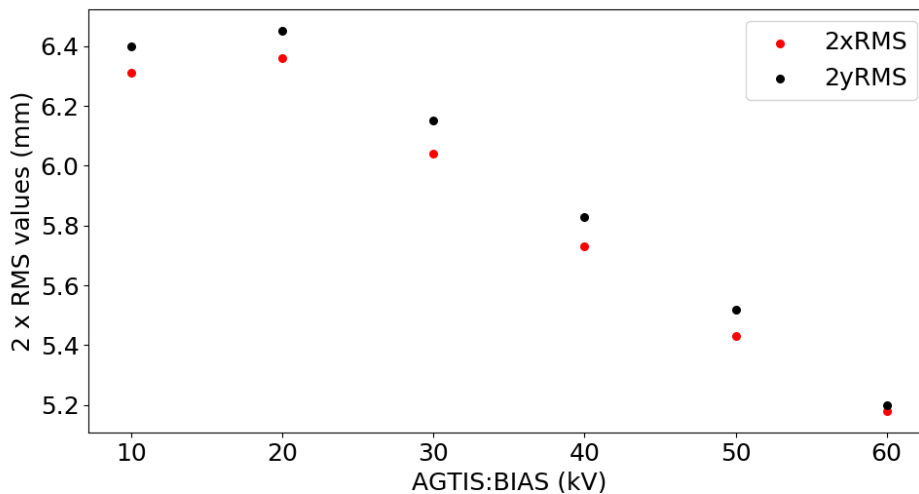
FIG. 6: $2 \times RMS$ and intensity values obtained after performing real space Tomography at location PM3 for beams with quadrupole values of Q1 = Q2 = Q3 = 0 V while varying source bias from 10-60 keV.

Phase-space Tomography

As was detailed previously, the first step in performing phase-space Tomography is to take multiple scans while varying the voltage of one quadrupole within the triplet. In this case, with the beam energy of the ion source set to 30 keV, the quadrupole Q1 is varied between 0 to 2400 V, with a scan taken every interval of 100 to 200 V. Once this is completed, Figure 7 is generated, plotting the $2{\times}RMS$ (sigma) squared values in each plane for every scan as a function of the quadrupole voltage. In this case we see that both in the x and y planes there is an approximate parabolic shape as well as a clear minimum value, therefore these chosen ranges are acceptable to be used for Tomography reconstruction. The Tomography outputs for the 30 keV beam case are presented in Figures 8-11.
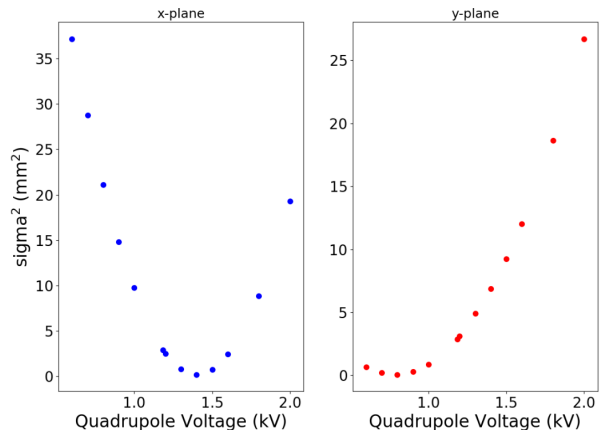
FIG. 7: Scans of 30 keV beam at location AGTIS:PM3; Q1 varied from 0 to 2400 V, Q2 = 1800V, Q3 = 1260V. Sigma^2 vs Q1 voltage for both x and y planes. Parabolic shape and clear minima present.
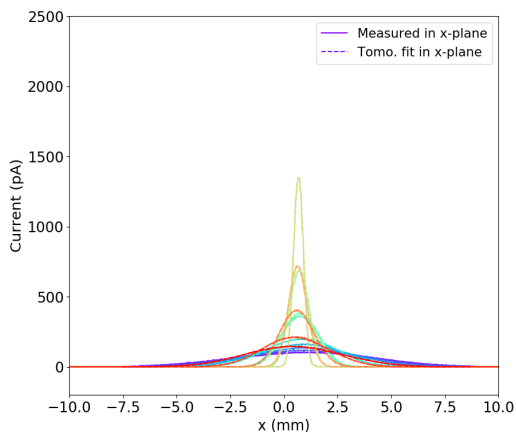
FIG. 8: Measured profiles (input) with MENT fit profiles (output) for x-plane phase-space.
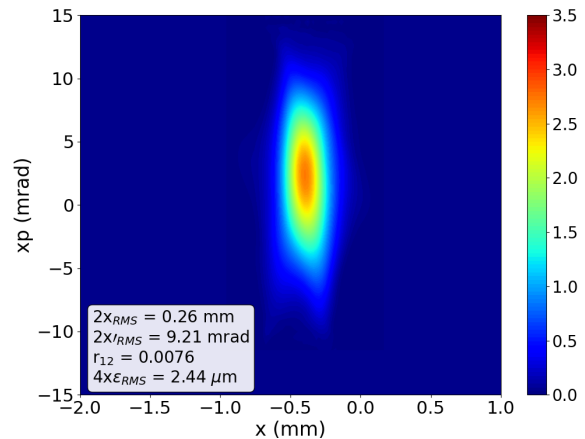
FIG. 9: Phase-space Tomography in the x-plane at the lohcation of the ion source extraction exit for 30 keV beams.
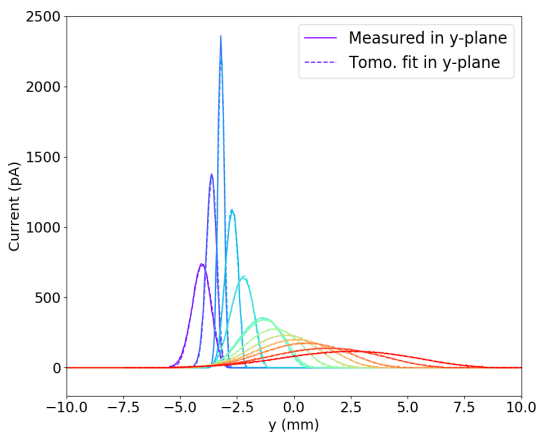
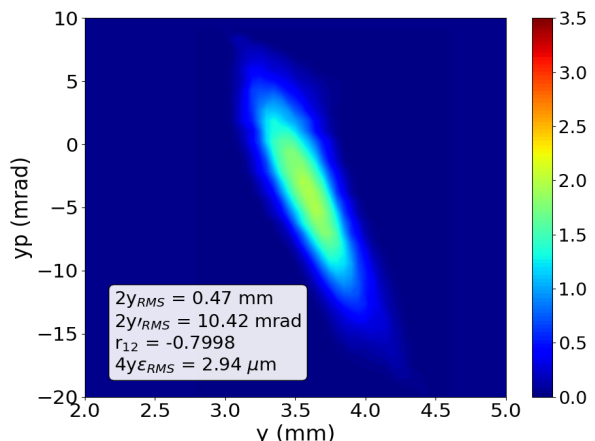FIG. 10: Measured profiles (input) with MENT fit profiles (output) for y-plane phase-space.

FIG. 11: Phase-space Tomography in the y-plane at the location of the ion source extraction exit for 30 keV beams.

An important parameter that is obtained from phase-space Tomography is the emittance, which represents the area that the beam occupies in phase space. The 4×RMS emittance formula can be described as follows:

$$4 \times \epsilon_{RMS} = 4 \times \sqrt{(x^2)(x\prime^2) - (xx\prime)^2}. \tag{1}$$

This parameter is invariant in the absence of external forces, thus is useful when trying to detect the possible presence of aberrations. One method used to benchmark the emittance estimated from the Tomography is by fitting the data points from Figure 7 to a parabola using a beam optics model coded in TRANSOPTR. By inputting the $2 \times RMS$ values along with their corresponding quadrupole values into TRANSOPTR while fixing the emittance parameter to the estimated values from Tomography, we can observe whether or not the fit that is output matches the initial data points. This plot is shown below in Figure 12.
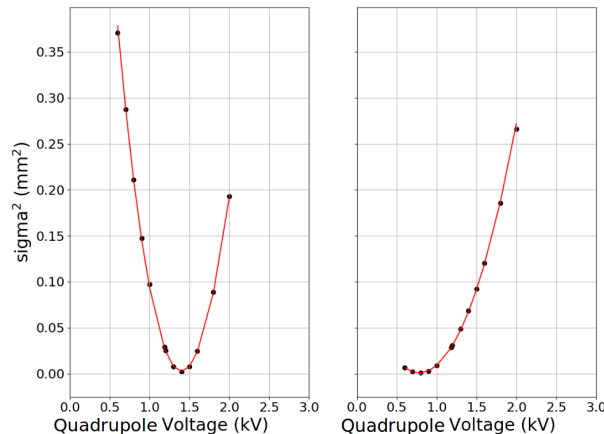
FIG. 12: TRANSOPTR fit of sigma^2 values for 30 keV beams.

It is evident from this plot that the TRANSOPTR fit in both the x and y planes matches the data very well, therefore the emittance values estimated from Tomography are are a good approximation.

Once the source is ramped up to its maximum energy of 60 keV, the process of phase-space Tomography is repeated. An important note for when taking the scans for this case; as the beam energy is being doubled, it is necessary to also double the quadrupole values, both for the quadrupole that is varied and the ones kept constant. The rotation matrix files must also be redone taking into account these new voltage values. Once all of this is assembled, the Tomography can be performed. The corresponding plots for phase-space Tomography at 60 keV can be found in the Appendix (Figures 25-26). It is important now to verify if the emittance is scaling according to the beam energy. This is done through the comparison of the normalized emittance, which is defined as follows:

$$\epsilon_N = \epsilon \beta \gamma \quad \text{where} \quad \beta = \frac{v}{c} \quad \text{and} \quad \gamma = \frac{1}{\sqrt{1 - \beta^2}} \tag{2}$$

The normalized emittance removes the dependence on beam energy, and should therefore be constant for different beam energies. To obtain the relativistic parameters (β and γ), the following equation is used:

$$qE = \frac{1}{2}mv^2 \tag{3}$$

Where q represents the ion's charge, E represents beam energy in electron volts (eV), and m represents atomic mass. In the case of our Cesium beam, q = 1 and m = 133 u, where the atomic mass unit u = 931.5×10^6eV/c^2. Plugging in these values we obtain:

$$E = \frac{1}{2} \times 133 \times 931.5 \times 10^6 \times \frac{1}{c^2}v^2 \Longleftrightarrow \frac{v}{c} = \sqrt{\frac{2E}{133 \times 931.5 \times 10^6}} = \beta \tag{4}$$

The above equation provides us with the value of β for each case when plugging in the energy value, and γ can be obtained from there. This computation is performed using the script *Calculations.py*. Table I presents the values for both the standard emittance, as well as the computed normalized emittance for each plane.

Beam Energy	ϵ_x	ϵ_y	ϵ_{Nx}	ϵ_{Ny}
30 keV	2.44 μm	2.94 μm	0.00169 μm	0.00206 μm
60 keV	1.79 μm	2.23 μm	0.00176 μm	0.00221 μm

TABLE I: Comparison of the standard and normalized emittances for 30keV and 60keV source beams.

We can see from this table that the values for the normalized emittance in both x and y planes are quite similar for both the 30 keV and 60 keV cases. Thus we can conclude that the emittance is scaling correctly with respect to beam energy, and that the general behavior of the test ion source is what's expected.

RFQ STUDIES

The Radio Frequency Quadrupole installed in the CANREB beamline has the objective of cooling and bunching the beams passed through it; both processes are expected to improve the emittance, i.e. reduce its value. Preliminary studies were performed on the behavior of the emittance through the RFQ, notably comparing the case where the beam was cooled but not bunched (DC case) and the case where the beam was both cooled and bunched. A schematic of the RFQ can be found below in Figure 13.
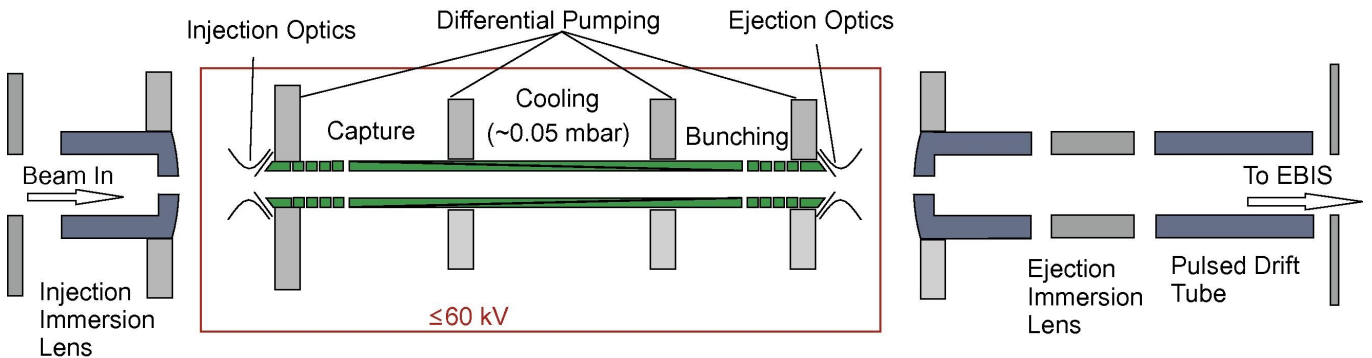
FIG. 13: Layout of the CANREB RFQ [5].

Phase-space Tomography was performed using measurements taken by LPM34 and reconstructed upstream to obtain the emittance of the beam at the exit of the RFQ. The Tomography contour plots for the DC and bunched cases can be seen below (additional plots can be found in the Appendix, Figures 31-38).
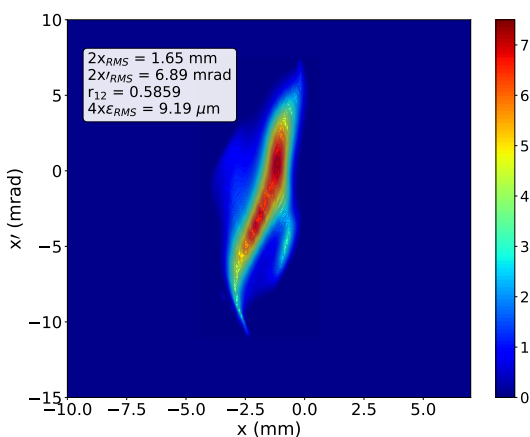
FIG. 14: Phase-space Tomography in the x-plane at the location of RFQ exit for DC beams.
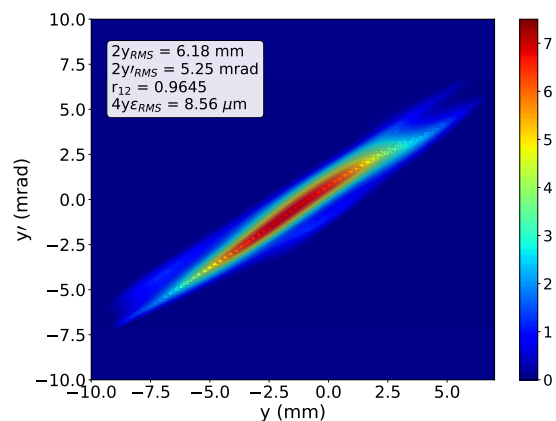
FIG. 15: Phase-space Tomography in the y-plane at the location of RFQ exit for DC beams.
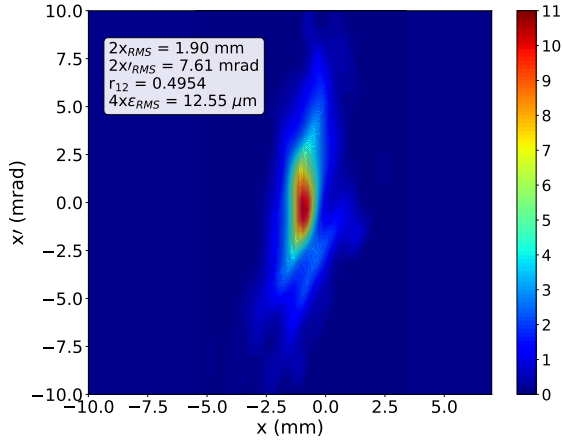
FIG. 16: Phase-space Tomography in the x-plane at the location of RFQ exit for bunched beams. Calculated $2 \times RMS$, angle and emittance values printed on figure.
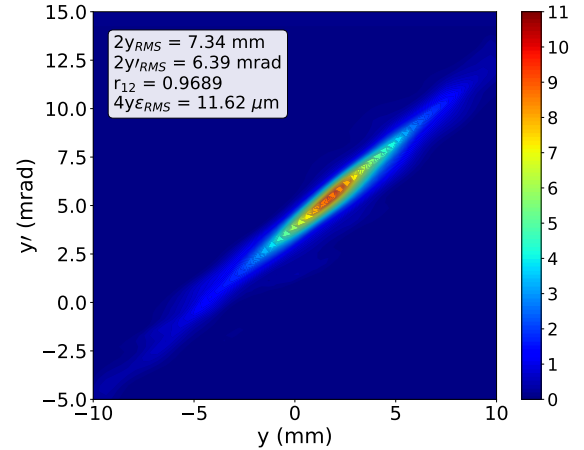

FIG. 17: Phase-space Tomography in the y-plane at the location of RFQ exit for bunched beams.

The contour plots presented above are much less clean cut than those seen in the previous section. There seem to be some distortions, particularly in the x plane for both cases, which could contribute to the higher emittances observed. Table II explicitly compares the emittances in the x and y plane for both cases. Contrary to what is expected, the emittance of the cooled and bunched beam is the highest of the two cases, and both cooled cases are much higher than the measured source emittance presented in the previous section. There are many processes occurring inside the RFQ, thus many factors could be influencing these results, notable the gas pressure, the timing of the trap, etc. Further systematic studies should be performed to get a better outlook on the performance of this particular machine element. Plans are in place for a new emittance scanner just downstream of the RFQ exit, which should help clarify what is taking place.

Beam Type	ϵ_x	ϵ_y
DC	9.19 μm	8.56 μm
Bunched	12.55 μm	11.62 μm

TABLE II: Comparison of the emittance through the RFQ for DC vs bunched beams.

FARADAY CUP STUDIES

An important measurement tool used to assist in the previous two studies is the Faraday Cup, a device which measures the current of the beams. These are typically located right next to the profile monitors along the beamline. Throughout commissioning however it was observed that in certain instances the current readings, particularly on FC3, were fluctuating even though the beams were entirely within the accepted aperture. This effect is investigated further in this section, comparing measurements from the Faraday cups located at FC3 and FC34.
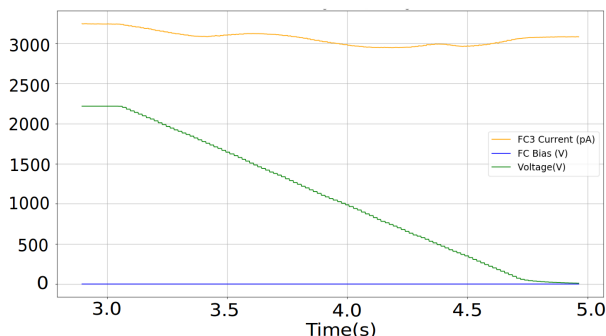

FIG. 18: Faraday cup FC3 current, bias voltage and Q3 voltage as a function of time. Bias Voltage fixed at 0 V. Clear variations in the FC3 current as the quadrupole voltage is changed.
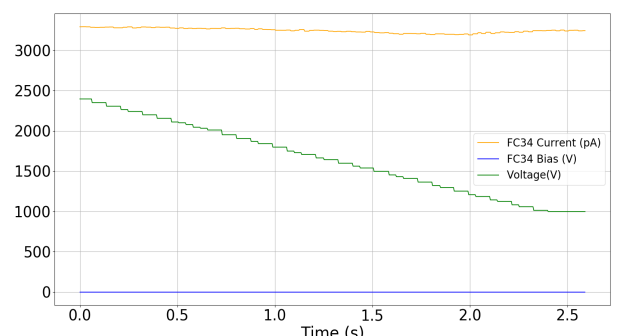

FIG. 19: Faraday cup FC34 current, bias voltage and Q34 voltage as a function of time. Bias Voltage fixed at 0 V. Less evident current variations as the quadrupole voltage is changed.

Figures 18 and 19 show the measurements performed on cups FC3 and FC34 respectively. Right away from Figure 18 one can observe the strange variations in the Faraday cup current. Real space Tomography verified that the size of the beam was within the accepted aperture (27 cm diameter cup), so this behavior is unexpected. Initially it was suspected this behavior was unique to that particular Faraday Cup, therefore these measurements were repeated for FC34 (Figure 19); there are visibly less variations, although they are still present (see additional plots in Appendix for more information, Figures 39-42). An initial hypothesis was that the Faraday Cups were perhaps not capturing all of the secondary electrons properly, therefore a negative bias of 50 V was added, and the measurements were retaken. Table III presents a comparison of these results.

Faraday Cup	0V Bias		50V Bias	
	Variation	Percent Variation	Variation	Percent Variation
FC3	300 pA	9.7%	95 pA	8.3%
FC34	100 pA	3.0%	35 pA	2.5%

TABLE III: Comparison of current fluctuations measured at FC3 and FC34 for Bias Voltages of 0 and 50 V respectively.

This table shows that the current fluctuations, while more pronounced for FC3, are still present for FC34. Furthermore, the addition of a negative bias does seem to reduce the variations somewhat, but does not eliminate them completely. Next, the geometry of the cups were studied by this time fixing the Quadrupole value to a fixed amount and varying the Bias voltage applied. These results are shown in Figures 20-21.
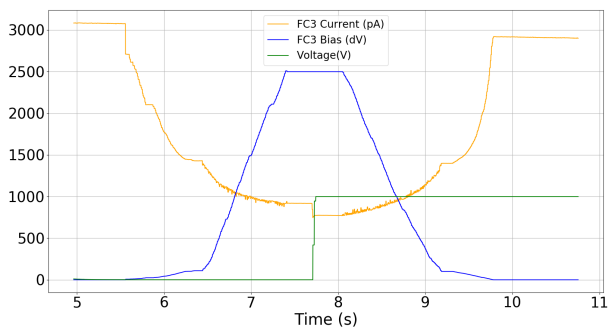
FIG. 20: Faraday cup FC3 current, bias voltage and Q3 voltage as a function of time. Quadrupole voltage first kept constant at 0 V, then changed to 1000 V.
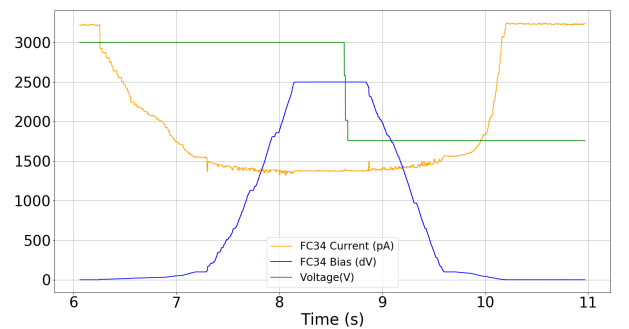
FIG. 21: Faraday cup FC34 current, bias voltage and Q34 voltage as a function of time. Quadrupole voltage first kept constant at 3000 V, then changed to 1750 V.

In both cases Q3's value is initially fixed at some chosen voltage as the bias voltage on the Faraday cup is varied. Once it reaches its maximum possible bias, the voltage of the quadrupole is changed to another chosen value, and this scan is repeated. In the case of an optimal Faraday cup geometry, these two scans should appear symmetric, as they do in Figure 21 for the case of FC34. In the case of FC3 however, Figure 20 shows a clear dip in the current reading as soon as the voltage of the quadrupole is changed, indicating a lack of symmetry.

Recently the area of the beamline around the Test Ion Source has been disassembled, as the source is being moved to the B2 level of the ARIEL Facility. During this process the Faraday cup FC3 was removed, and it was discovered that its bias ring was offset, potentially contributing to unusual behaviour. However, the fact that this behavior was still present, although to a lesser degree, at FC34, leads one to believe that this may be a problem present throughout all the Faraday Cups not only in the CANREB beamline, but potentially in the ISAC facility as well. It would thus be advisable to repeat these measurements at multiple other locations, not only within ARIEL but also ISAC, to verify whether or not this is a recurring issue.

CONCLUSION

This project ultimately determines that the technique of Tomography reconstruction in CANREB is effective for visualizing the beams inside the beamline and determining their emittance. The behavior of the test ion source is as expected, with the emittance scaling appropriately with beam energy. Additional systematic studies are recommended

for the CANREB RFQ, as well as for the Faraday cups throughout ARIEL and ISAC. The commissioning of the CARNEB beamline will continue, with the next step being to commission beam through the High Resolution Mass Separator in the B2 level of ARIEL.

ACKNOWLEDGMENTS

[1] F. Ames et al., *The CANREB Project for Charge State Breeding at TRIUMF*, 17th International Conference on Ion Sources, CERN, Geneva, October, 2017.

[2] Y. N. Rao and R. Baartman, *Transverse phase-space Tomography in TRIUMF injection beamline*, Proceedings of IPAC2011, San Sebastian, Spain, pp. 1144-1146.

[3] S. Saminathan, *ARIEL Test Ion Source*, TRIUMF, Vancouver, Canada, Internal report, TRI-DN-16-35, September, 2017.

[4] O. Lailey, *TOMOGRAPHY RECONSTRUCTION FOR ARIEL CANREB BEAM COMMISSIONING*, TRIUMF, Vancouver, Canada, Internal Report, TRI-BN-19-07, 2019.

[5] B.R.Barquest, J.C.Bale, J.Dilling, G.Gwinner, R.Kanungo, R.Krcken, M.R.Pearson *Development of a new RFQ beam cooler and buncher for the CANREB project at TRIUMF*, Nuclear Instruments and Methods in Physics Research Section B: Beam Interactions with Materials and Atoms, Volume 376, 2016.

APPENDIX

AGTIS_PM3_20190712_1217
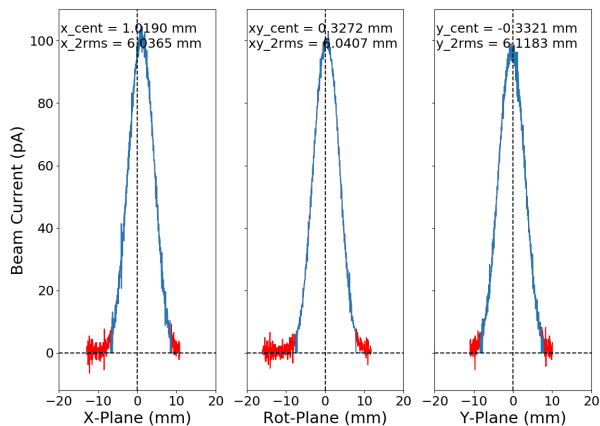
FIG. 22: Profile scan taken at AGTIS:PM3 for beam with AGTIS:Bias of 30keV, quadrupoles Q1, Q2 and Q3 set to 0V. Raw data plotted in red and data having undergone noise filtering plotted in blue.
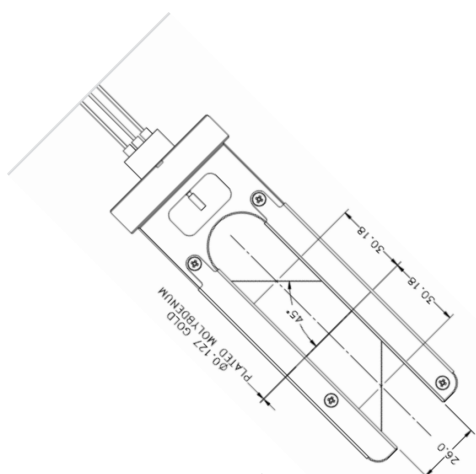
FIG. 23: Profile Monitor AGTIS:PM3 consisting of three wires which measure the vertical, horizontal and rotational planes respectively.
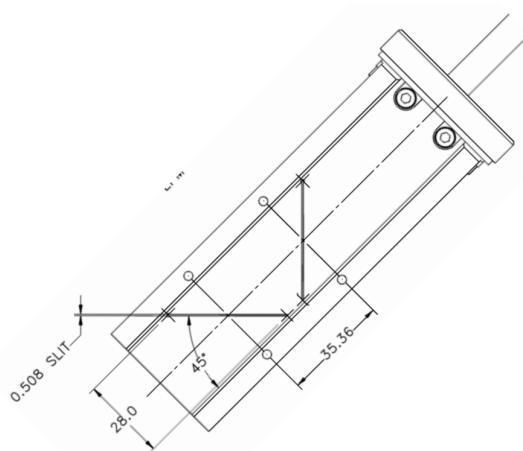
FIG. 24: Linear Profile Monitor AGTE:LPM23 consisting of two slits which measure the vertical and horizontal plane respectively.

60 keV plots
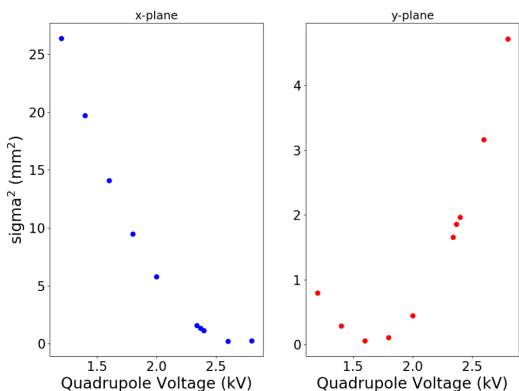
FIG. 25: Scans of 60 keV beams at location AGTIS:PM3, Q1 varied from 0 to 4000 V, Q2 = 3600 V, Q3 = 2520 V. Sigma^2 vs Q1 voltage for both x and y planes. Parabolic shape and clear minima present.
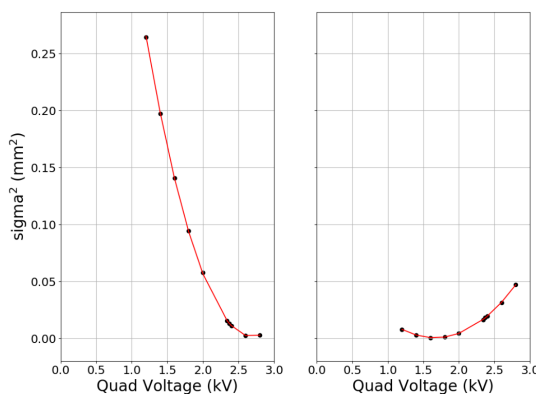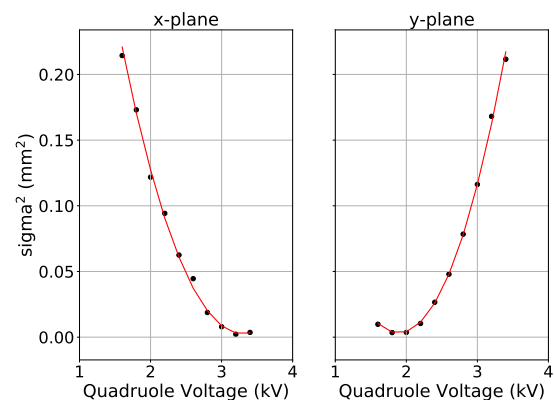

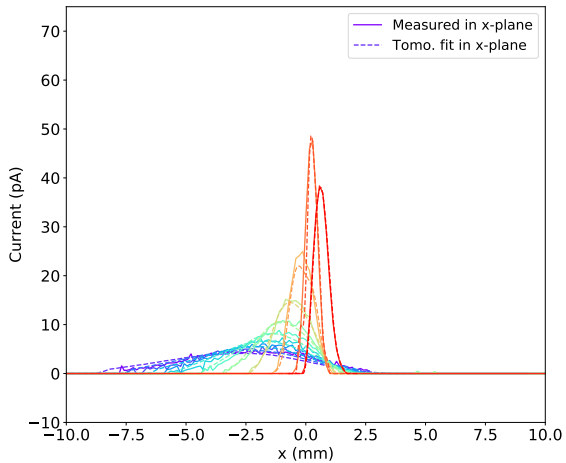FIG. 26: TRANSOPTR fit of sigma^2 values for 60 keV beams.
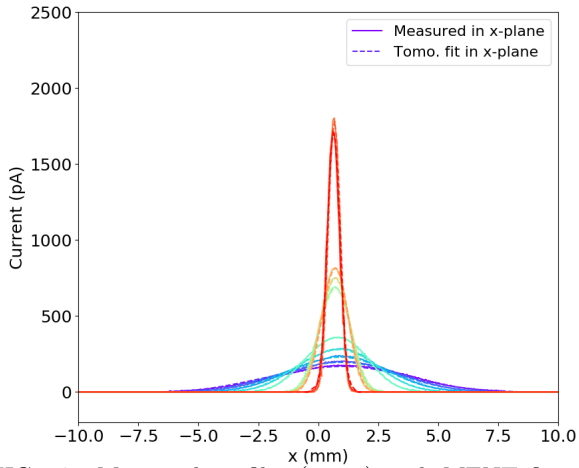
FIG. 27: Measured profiles (input) with MENT fit profiles (output) for x-plane phase-space.
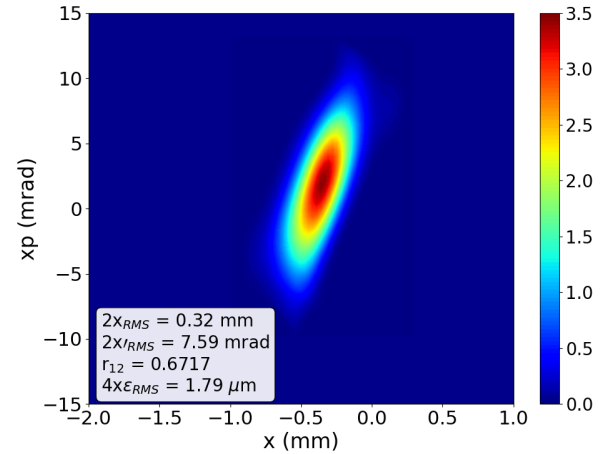
FIG. 28: Phase-space Tomography in the x-plane at the location of the ion source extraction exit for 60 keV.
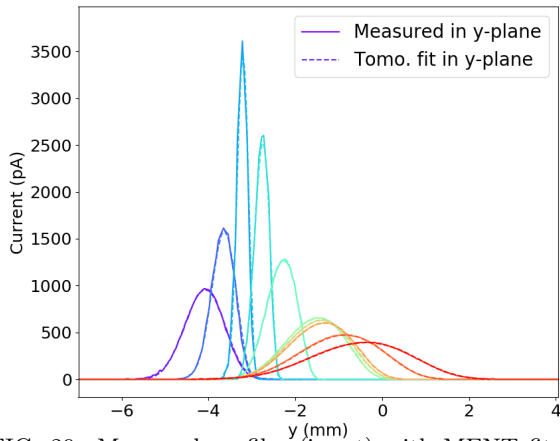
FIG. 29: Measured profiles (input) with MENT fit profiles (output) for y-plane phase-space.
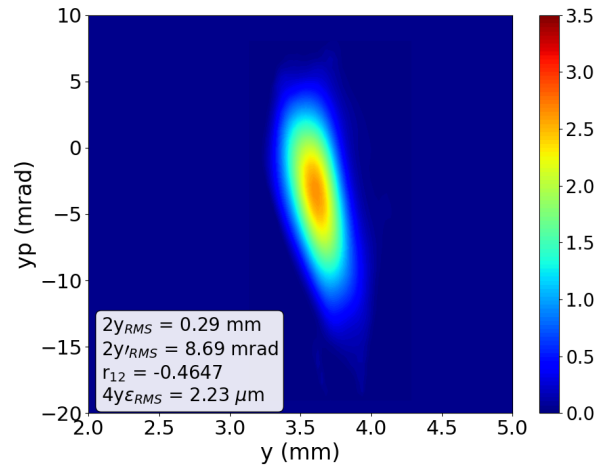
FIG. 30: Phase-space Tomography in the y-plane at the location of the ion source extraction exit for 60 keV.

DC plots
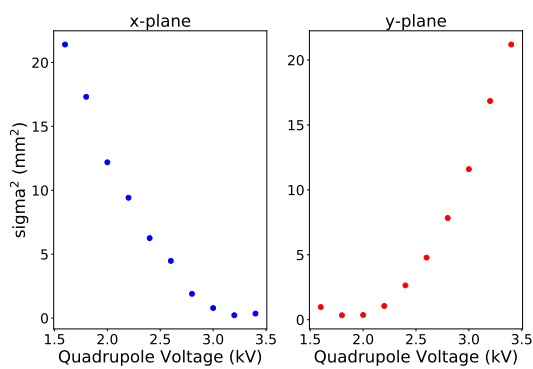
FIG. 31: Scans of 30 keV DC beams at location AGTE:LPM34, Q34 varied from 1000 to 4000 V, Q32 = 300 V, Q33 = 1406 V. Sigma^2 vs Q34 voltage for both x and y planes. Parabolic shape and clear minima present.

FIG. 32: TRANSOPTR fit of sigma^2 values for DC beams.

FIG. 33: Measured profiles (input) with MENT fit profiles (output) for x-plane phase-space DC beams.
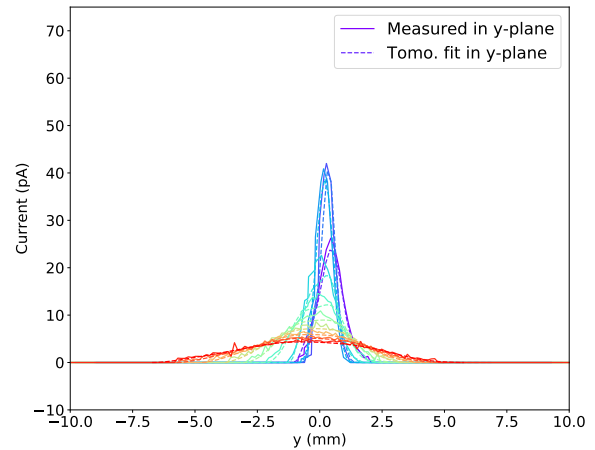
FIG. 34: Measured profiles (input) with MENT fit profiles (output) for y-plane phase-space DC beams.
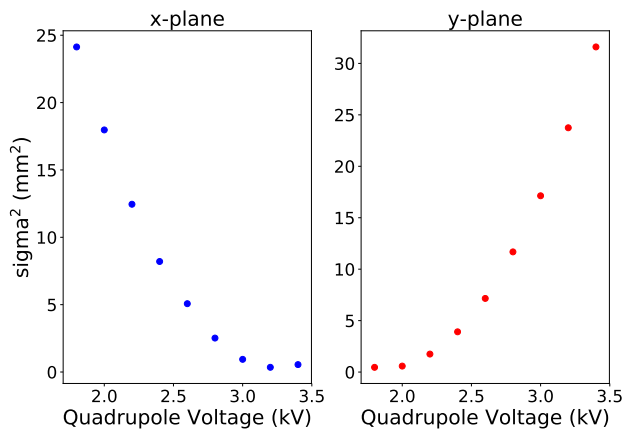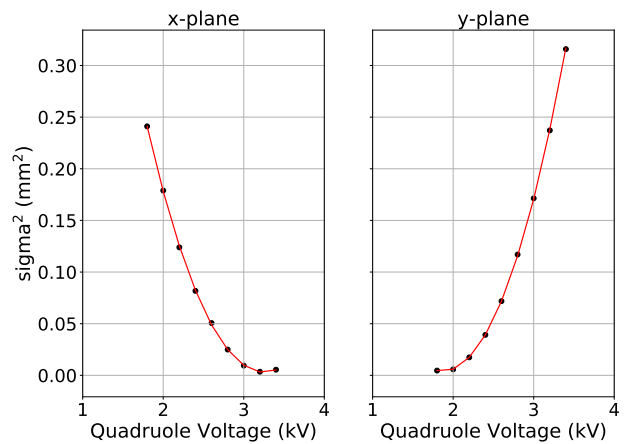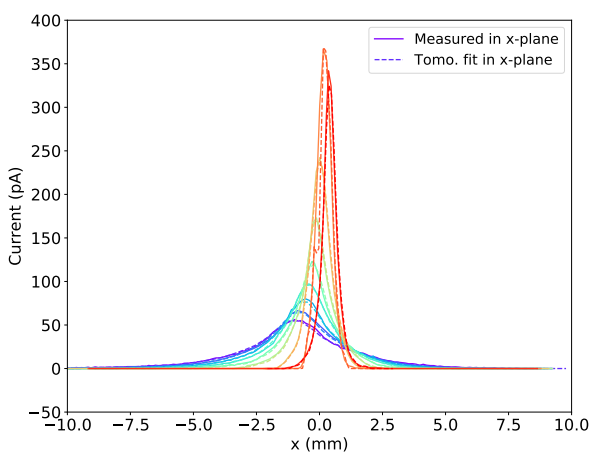
Bunched plots

FIG. 35: Scans of 30 keV bunched beams at location AGTE:LPM34, Q34 varied from 1000 to 4000 V, Q32 = 300 V, Q33 = 1406 V. Sigma^2 vs Q34 voltage for both x and y planes. Parabolic shape and clear minima present.

FIG. 36: TRANSOPTR fit of sigma^2 values for bunched beams.

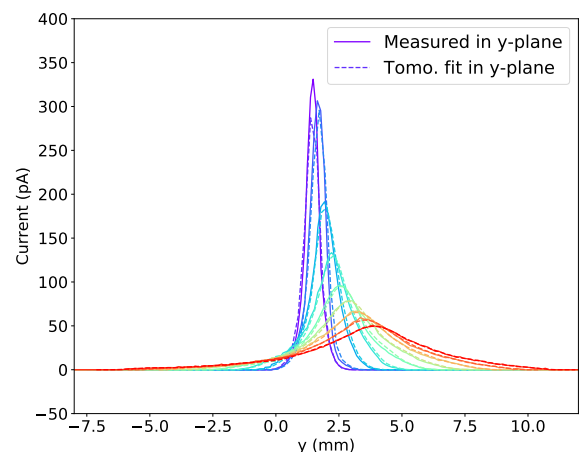FIG. 37: Measured profiles (input) with MENT fit profiles (output) for x-plane phase-space bunched beams.

FIG. 38: Measured profiles (input) with MENT fit profiles (output) for y-plane phase-space bunched beams.
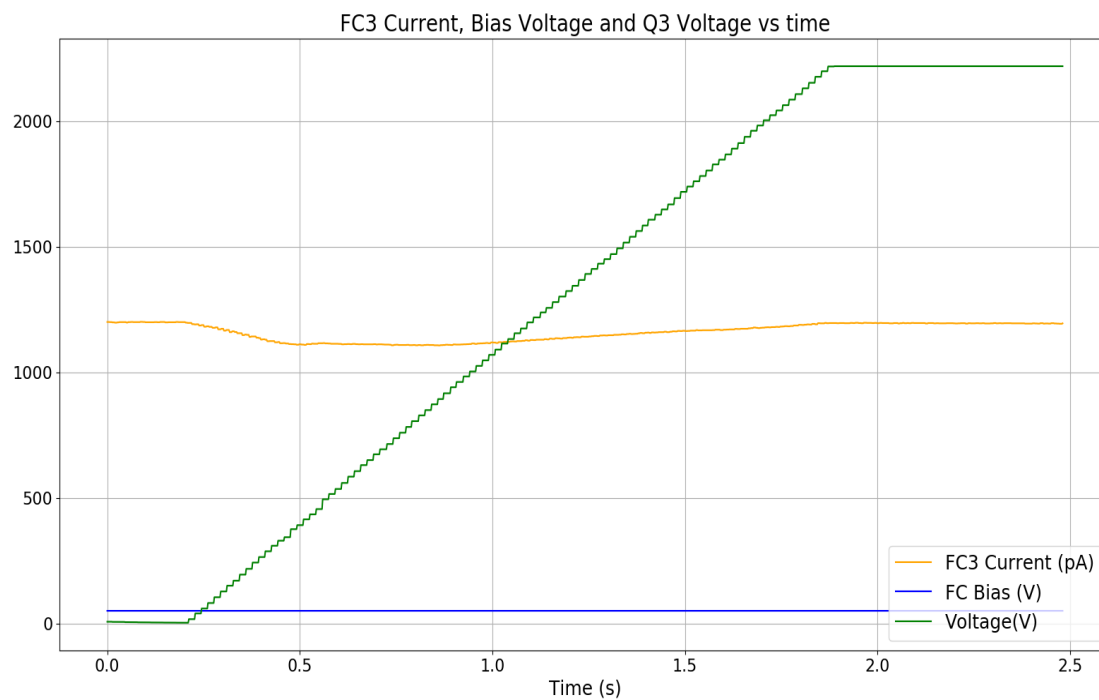
Faraday Cup plots

FIG. 39: Faraday cup FC3 current, bias voltage and Q3 voltage as a function of time. Bias voltage fixed to 50 V. Clear dip in FC3 current as the quadrupole voltage is changed.
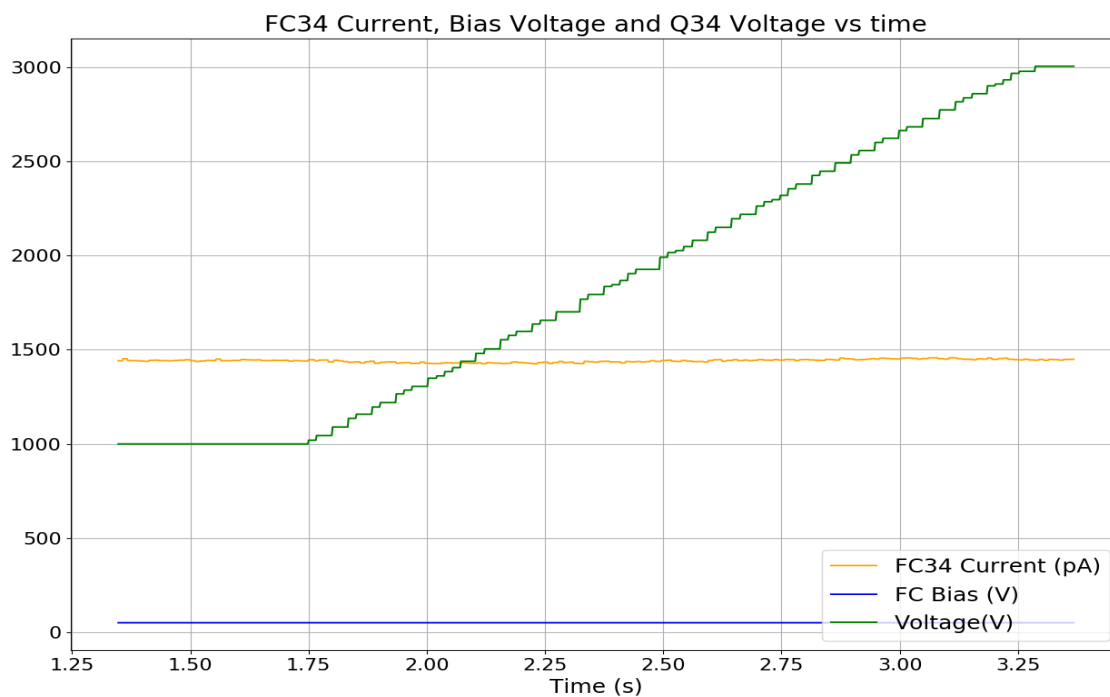

FIG. 40: Faraday cup FC34 current, bias voltage and Q34 voltage as a function of time. Bias voltage fixed at 50 V. Less evident current fluctuations as the quadrupole voltage is changed.
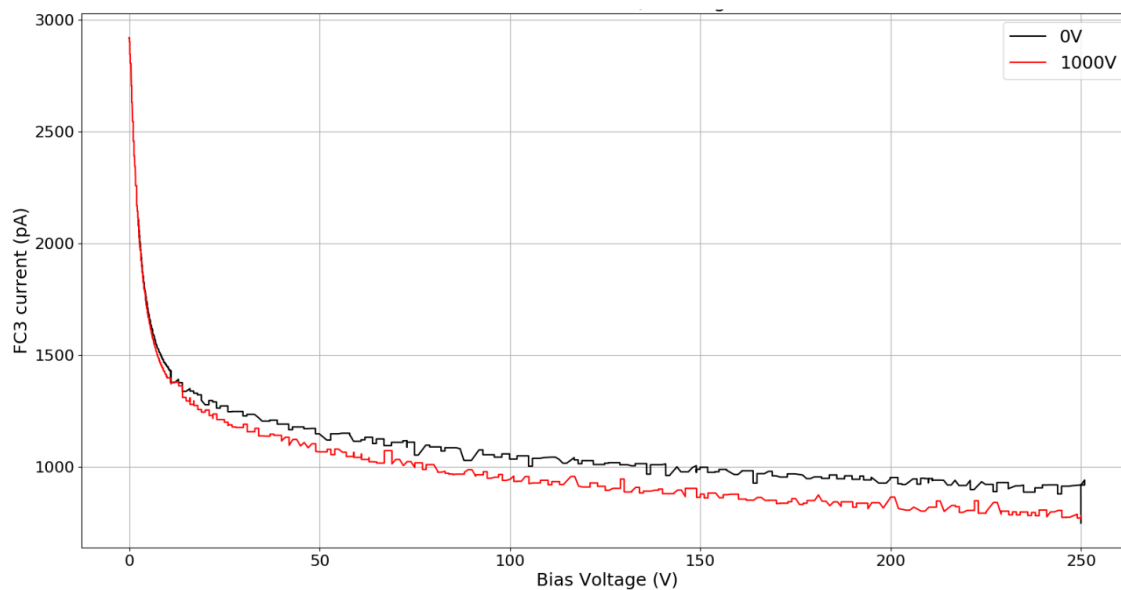
FIG. 41: FC3 Current as a function of its bias voltage for consecutive scans, first with Q3 set to 0 V then set to 1000 V. Obvious lack of symmetry between the two scans, indicating a clear issue with Faraday cup geometry.
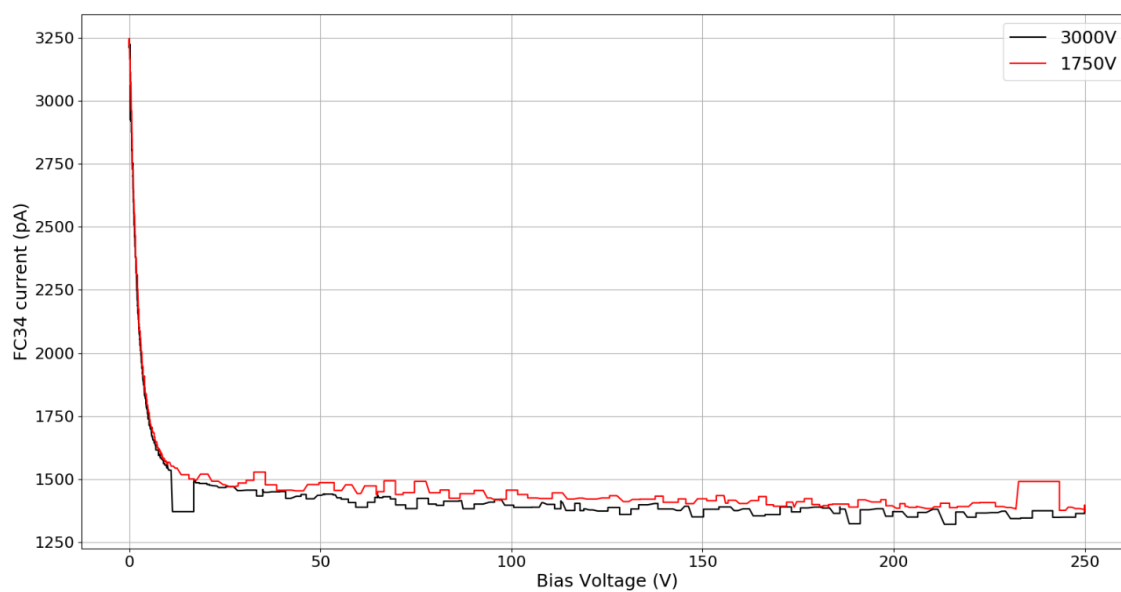

FIG. 42: FC34 current as a function of its bias voltage for consecutive scans, first with Q34 set to 3000 V then set to 1750 V. Slight lack of symmetry between the two scans, with red curve consistently being above black curve, indicating a possible issue with Faraday cup geometry.